31st Annual International Conference of the IEEE EMBS
Minneapolis, Minnesota, USA, September 2-6, 2009

Towards A Genioglossus Surface EMG Model of Obstructive Sleep Apnea

Eric C-P Chua, David G McSharry, Walter T McNicholas and Madeleine M Lowery

Abstract— **The behaviour and activity of the genioglossus muscle during sleep is of considerable interest to investigators of obstructive sleep apnea syndrome. Therefore, we contribute an model of genioglossus EMG activity during breathing, based on recent physiological findings. We present the modelling techniques and simulation results. The model incorporates new data on fibre type, motor unit type and motor unit firing characteristics. Although we report its use for modelling genioglossus surface EMG, this model can be used to simulate both genioglossus surface and intramuscular EMGs of various electrode configurations. We also discuss the simulation results in the context of the limited experimental data available for surface genioglossus EMG in obstructive sleep apnea.**

I. Introduction

Obstructive sleep apnea syndrome (OSAS) is a highly prevalent but under-diagnosed condition. Left untreated, OSAS is associated with serious cardiovascular consequences [1], and treatment has been shown to significantly reduce these risks [2].

OSAS is associated with an increased collapsibility of the upper airway, and the genioglossus (GG) muscle is thought to be the main contributor towards maintenance of upper airway patency [3]. GG electromyography (EMG), including both surface and intramuscular techniques, is therefore important for investigating OSAS, as it allows us to understand and monitor the behaviour and activity of the GG muscle. Surface EMG offers an advantage of being less invasive, and is a potential platform for developing novel diagnostic or therapeutic strategies. An GG surface EMG model would therefore be very useful, such as for aiding experimental data interpretation [4], or for exploring electrical stimulation as a therapeutic strategy [5].

In this study we present a model of genioglossus EMG activity during breathing. This model is based on the one presented by O'Connor *et al* [6], and is updated in terms of fibre type, motor unit type and motor unit firing characteristics by incorporating recent physiological findings. The longer-term goal of this work is to develop an accurate GG surface EMG model of OSAS.

II. Method: Genioglossus EMG Model

A. Structure and Properties

The model consists of a pair of identical genioglossus muscles spaced 1 mm apart. Figure 1 illustrates the gross structure of one of the genioglossus muscles. Based on a simplification of known anatomy [7], the genioglossus muscles were modelled as fan-shaped structures with a rectangular cross-section at the anterior end. In a cadaver study, Saigusa *et al* found that Type II fibres were dominant anteriorly, while there was no dominant fibre type posteriorly [8]. In a canine study, Mu *et al* reported a ∼60/40 proportion of fast to slow twitch fibres anteriorly, and a ∼35/65 proportion posteriorly [7]. Accordingly, we partitioned our fan-shaped GG muscle into 2 components (Figure 1). The top two-thirds of the muscle is denoted the top component, while the bottom one-third is denoted the bottom component.

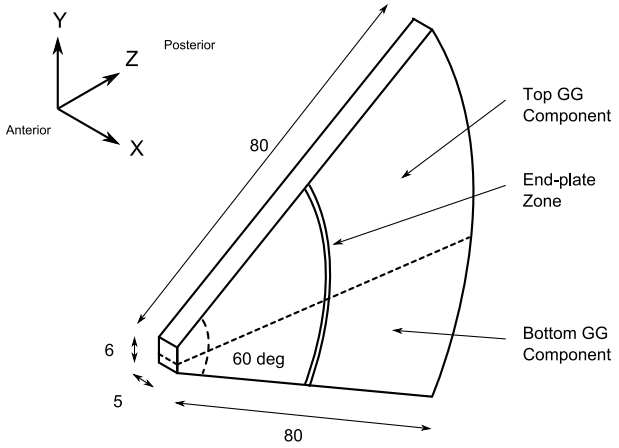

Fig. 1. Isometric drawing illustrating the gross structure of each simulated genioglossus muscle. Individual muscle fibres were simulated within this gross structure. All dimensions are in mm unless otherwise stated.

Each GG component comprised motor units of various sizes, determined by the number of component fibres (assuming constant fibre density). At the anterior end, each motor unit territory centre was randomly assigned a location within the rectangular boundary of the GG component, and motor unit territories were allowed to overlap.

Each motor unit was made up of muscle fibres of the same diameter and conduction velocity. At the anterior end, each fibre was randomly assigned a location within the circular cross-section of its parent motor unit. Each fibre was inclined at an angle proportional to its y-axis location at the anterior end so that the muscle fibres span the entire fan-shaped structure. The innervation point for each fibre was randomly located within the end-plate zone. All muscle fibres were of the same length.

Each motor unit was then assigned the number of component fibres, fibre diameter and fibre conduction velocity.

This work was supported in part by Science Foundation Ireland via the EEDSP Strategic Research Cluster, and in part by UCD seed funding to Chua and Lowery. Chua and Lowery are with University College Dublin, Ireland. McSharry and McNicholas are with St Vincent's University Hospital, Ireland. (madeleine.lowery@ucd.ie)

TABLE I

SIMULATION PARAMETERS

Parameter	Value
No of Motor Units	80 *
No of Fibres Per Motor Unit	40 – 150
Fibre Length	80 mm
Fibre Diameter	25 – 40 μm
Fibre Conduction Velocity	3.5 – 4.5 ms^{-1}
Fibre Density	20 mm^{-2}
End-Plate Zone Width	2 mm
Transmembrane Voltage ($V(z)$)	$96\ (2z)^3\ \exp(-2z) - 90$
Radial Extracellular Conductivity (σ_r)	0.063 mho/m
Axial Extracellular Conductivity (σ_z)	0.33 mho/m
Intracellular Conductivity (σ_{in})	1.01 mho/m
No of Action Potential Point Sources (N)	150
Length of Action Potential	15 mm

*: Per GG muscle, including both top and bottom components.

Based on the Saigusa [8] and Mu [7] studies, a greater proportion of Type II was assigned to the motor units in the top component than those in the bottom component. This was achieved by assigning the properties using convex quadratic polynomials in the top component, and linearly in the bottom component.

B. Motor Unit Action Potentials

Action potentials generated by each fibre were computed, and the motor unit action potential (MUAP) then obtained as the sum of individual action potentials.

When a fibre was activated, an action potential propagated with uniform conduction velocity away from the fibre end-plate towards each fibre end. The action potential was discretised into N point sources, Δz apart. When the point sources reached the fibre ends, they remained there until partially or wholly cancelled by later-arriving point sources.

The resulting voltage detected at a given electrode location was determined as follows. The muscle fibres were assumed to lie in an infinite, cylindrically anisotropic and homogenous volume conductor, with radial and axial conductivities denoted by σ_r and σ_z respectively. For a given electrode location and a given point source j on the fibre, let r denote the shortest distance from the electrode to the fibre, and z_j the distance of the point source along the fibre.

For each time step, the potential ϕ at the electrode was obtained using (Eq. 1) [9]

$$\phi = \frac{d^2\sigma_{in}}{16\sigma_r} \sum_{j=1}^{N} \frac{d^2V(z_j)}{dz^2} \frac{1}{\sqrt{\frac{\sigma_z}{\sigma_r} r^2 + z_j^2}} \Delta z \qquad (1)$$

where d is the fibre diameter, σ_{in} is the intracellular conductivity, and $V(z)$ is the transmembrane voltage. Table I details the specific simulation parameters.

C. Surface EMG

Individual firing times for each motor unit were assigned based on a discharge characteristics model (described later in Section II-C.2) and the computed MUAP was assumed to be generated each time that motor unit was activated.

TABLE II

ASSIGNMENT OF MOTOR UNITS

	Phasic	Tonic		
GG Component	IP	IT	TT	Total
Top	27 (51)	14 (26)	12 (23)	53
Bottom	7 (26)	11 (41)	9 (33)	27

Numbers in parenthesis indicate the percentage relative to the total number of motor units in that GG component.

The surface EMG was then obtained as the sum of these individual MUAP trains. One minute of paced breathing (12 breaths per minute) was simulated at 4000 Hz. The simulated GG surface EMG was also post-processed to provide comparison with experimental data in the literature. The EMG was first rectified, and the moving time average (MTA) EMG then obtained by numerically integrating the EMG using 100 ms, non-overlapping epochs [10].

1) Motor Unit Type and Anatomical Distribution: Saboisky *et al* [4] investigated GG single motor units in awake healthy adults during quiet breathing, and reported a more detailed motor unit classification beyond the traditional phasic and tonic types. Wilkinson *et al* [11] reported similar findings in a study of discharge patterns during sleep onset, although the distribution of motor units between the six motor unit types differed somewhat between the two studies. Accordingly, we modelled the three most common motor unit types reported, i.e. inspiratory phasic (IP), inspiratory tonic (IT), and tonic (TT). These motor units accounted for on average 82 % of single motor units studied. Briefly, inspiratory phasic motor units are only active during inspiration. Inspiratory tonic motor units are tonically active throughout respiration, and increase their activity during inspiration. Tonic motor units are tonically active throughout respiration.

In addition, Saboisky *et al* [4] reported an anatomical difference in the distribution of the different motor unit types. They found a ∼25/75 distribution between phasic and tonic motor units posteriorly, and an approximately equal distribution anteriorly. Based on these data on motor unit type and anatomical distribution, we assigned the simulated motor units in each GG component to the three motor unit types (Table II). Motor units were assigned to inspiratory tonic, tonic and inspiratory phasic types in ascending order of motor unit size.

2) Discharge Characteristics: Saboisky *et al* [4] also reported experimental data on the discharge statistics of various motor unit types. These findings were incorporated to simulate individual discharge times for each motor unit. Briefly, for inspiratory phasic motor units, 28 % of motor units commenced firing before inspiratory onset, and 72 % finished firing by 3/4 of inspiration. The mean onset and peak firing frequencies reported were 10.3 and 15.0 Hz respectively. For inspiratory *tonic* motor units, 62 % of motor units commenced firing before inspiratory onset, and firing continued until the end of expiration. The mean onset and peak firing frequencies reported were 16.5 and 24.7 Hz respectively. For tonic motor units, the average firing

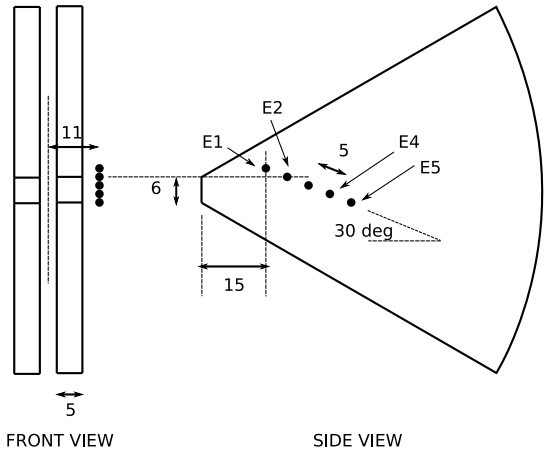

Fig. 2. Orthographic drawing depicting simulated electrode locations relative to the GG muscles. Only the electrode array medial to the left GG muscle is shown. All dimensions are in mm unless otherwise stated.

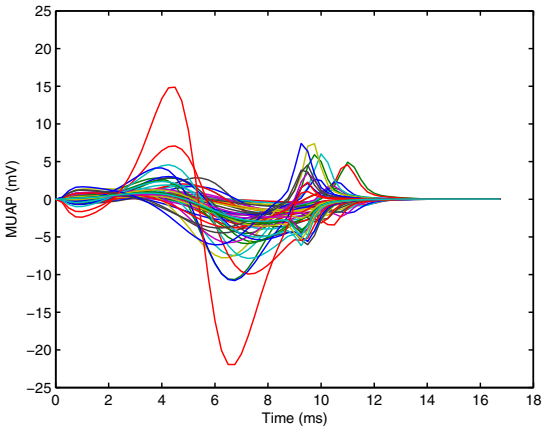

Fig. 3. Example of individual motor unit action potentials (MUAP), obtained using a bipolar configuration. MUAPs were computed as the sum of simulated individual fibre action potentials.

frequency reported was 19.5 Hz.

For phasic activity, the motor units were simulated to discharge in accordance with the 'onion skin' phenomenon [12], i.e. smaller motor units were recruited earlier, and attained a higher peak firing rate. Motor unit recruitment and discharge time determination was based on the Fuglevand model [13]. Based on data presented in the Saboisky study [4], we used a log function to determine recruitment threshold excitation. In keeping with the size principle [14], motor units of the same type in both the top and bottom GG components were arranged in ascending order of size, and assigned firing characteristics starting from the one with the lowest firing frequencies.

D. Electrode Configuration

The electrode simulated is an improved version of that proposed by O'Connor *et al* [6]. Briefly, the device is an intraoral surface electrode, and is made up of two parallel arrays of five point electrodes (Figure 2). The parallel arrays are co-located on the left side of the mid-line of the mouth, just lateral to the left GG muscle, and are oriented parallel to the muscle fibres. Bipolar surface EMG measurements were simulated for 2 electrode pairs (E1-E2 and E4-E5, Figure 2).

III. Results

To recap, the proposed model a) computes the motor unit action potentials (MUAP) of individual motor units, b) generates the discharge times of each motor unit. The surface EMG at each point in time is then obtained as the sum of active action potentials.

A. Motor Unit Action Potentials

Figure 3 gives an example of the computed individual motor unit action potentials (MUAP). The MUAPs were dominated by the propagating part of the action potential waveform and an attenuated end-effect component, due to extinction of the action potential at the musculotendonous junction, may also be seen.

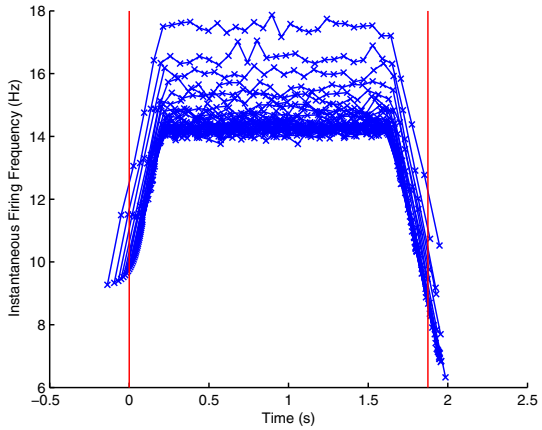

Fig. 4. Discharge times of simulated inspiratory phasic motor units ($N = 34$). Timings are shown for 1 inspiratory cycle, with each line representing the timings for one motor unit. Actual discharge times are marked with crosses. The vertical lines mark the start and 75 %-point of inspiration.

B. Discharge Characteristics

An example of the simulated discharge times is shown in Figure 4. As shown, the discharge times were consistent with the 'onion skin' phenomenon [12], and the proportion of motor units commencing and stopping firing relative to the inspiratory cycle agreed closely with experimental findings from the Saboisky study.

C. Surface EMG

Figure 5 shows examples of the resultant simulated surface EMG signal (at the E1-E2 electrode pair; see Figure 2 for electrode location). Figure 5(a) shows a 30-second segment, while Figure 5(b) shows the same segment after rectification and averaging (see Section II-C for details). As shown, a strong phasic component was evident during inspiration. This was contributed by a) the inspiratory phasic motor units, which were active only during inspiration, and b) the inspiratory tonic motor units, which increased their activity

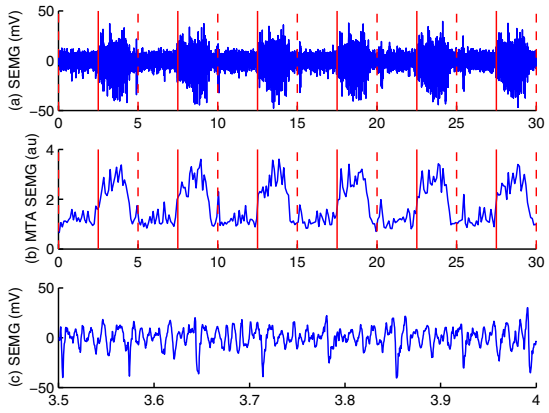

Fig. 5. Simulated bipolar surface EMG obtained from the E1-E2 electrode pair. (a) Thirty-second segment. Bold lines: Inspiration onset. Dotted lines: Expiration onset. (b) Corresponding moving-time averaged surface EMG. (c) Half-second mid-inspiratory segment from (a) (T = 3.5 to 4 s).

during inspiration. Figure 5(c) zooms into a half-second, mid-inspiratory segment from (a). Qualitatively similar results were obtained with the E4-E5 electrode pair.

IV. Discussion

In this study, a model of GG EMG activity during breathing was developed. The model incorporates recent findings regarding motor unit discharge statistics and distribution of motor units according to type. This model could potentially be useful for applications such as investigating respiratory drive changes or examining EMG changes during apnea.

The simulation results indicated strong inspiratory phasic activity. This finding is consistent with previous surface EMG work in children. Katz *et al* [10] measured surface genioglossus EMG from healthy children and children with OSAS using the Doble electrode [15]. In healthy children, they did not observe phasic activity during inspiration, but were able to do so in children with OSAS, and the level of inspiratory phasic activity correlated positively with disease severity. These results suggest that the current model could be suitable for modelling surface EMG activity in subjects with OSAS. Furthermore, the current electrode has improved selectivity over the Doble electrode, achieved by a much smaller inter-electrode distance and lower impedance. This potentially allows it to better detect phasic surface EMG activity. Work is currently on-going to use the proposed electrode to measure surface EMG activity in adults with suspected OSAS during sleep.

We did not model the expiratory phasic and expiratory tonic motor unit types reported in the Saboisky study [4]. These motor units would have contributed phasic activity during expiration and hence at least partially mask the inspiratory phasic activity. However, these motor units were rather rare, and were therefore not simulated. They made up on average 14 % of single motor units investigated in the Saboisky [4] and Wilkinson [11] studies, and were found only in ∼25 % of subjects.

References

[1] W. McNicholas, M. Bonsignore, and the Management Committee of EU COST ACTION B26, "Sleep apnoea as an independent risk factor for cardiovascular disease: current evidence, basic mechanisms and research priorities," *Eur Respir J*, vol. 29, pp. 156–78, 2007.

[2] L. S. Doherty, J. L. Kiely, V. Swan, and W. T. McNicholas, "Long-term effects of nasal continuous positive airway pressure therapy on cardiovascular outcomes in sleep apnea syndrome," *Chest*, vol. 127, no. 6, pp. 2076–2084, June 2005.

[3] J. Remmers, W. deGroot, E. Sauerland, and A. Anch, "Pathogenesis of upper airway occlusion during sleep," *J Appl Physiol*, vol. 44, no. 6, pp. 931–8, 1978.

[4] J. Saboisky, J. Butler, R. Fogel, J. Taylor, J. Trinder, D. White, and S. Gandevia, "Tonic and phasic respiratory drives to human genioglossus motoneurons during breathing," *J Neurophysiol*, vol. 95, no. 4, pp. 2213–21, 2006.

[5] A. Schwartz, M. Bennett, P. Smith, W. De Backer, J. Hedner, A. Boudewyns, P. Van de Heyning, H. Ejnell, W. Hochban, L. Knaack, *et al.*, "Therapeutic electrical stimulation of the hypoglossal nerve in obstructive sleep apnea," *Arch Otolaryngol Head Neck Surg*, vol. 127, no. 10, pp. 1216–23, 2001.

[6] C. O'Connor, M. Lowery, L. Doherty, M. McHugh, C. O'Muircheartaigh, J. Cullen, P. Nolan, W. McNicholas, and M. O'Malley, "Improved surface emg electrode for measuring genioglossus muscle activity," *Respir Physiol Neurobiol*, vol. 159, no. 1, pp. 55–67, 2007.

[7] L. Mu and I. Sanders, "Neuromuscular specializations of the pharyngeal dilator muscles: Ii. compartmentalization of the canine genioglossus muscle," *Anat Rec*, vol. 260, no. 3, pp. 308–25, 2000.

[8] H. Saigusa, S. Niimi, K. Yamashita, T. Gotoh, and M. Kumada, "Morphological and histochemical studies of the genioglossus muscle," *Ann Otol Rhinol Laryngol*, vol. 110, no. 8, pp. 779–84, 2001.

[9] M. Lowery, C. Vaughan, P. Nolan, and M. O'Malley, "Spectral compression of the electromyographic signal due to decreasing muscle fiber conduction velocity," *IEEE Trans Rehabil Eng*, vol. 8, no. 3, pp. 353–61, 2000.

[10] E. Katz and D. White, "Genioglossus activity during sleep in normal control subjects and children with obstructive sleep apnea," *Am J Respir Crit Care Med*, vol. 170, no. 5, pp. 553–60, 2004.

[11] V. Wilkinson, A. Malhotra, C. Nicholas, C. Worsnop, A. Jordan, J. Butler, J. Saboisky, S. Gandevia, D. White, and J. Trinder, "Discharge patterns of human genioglossus motor units during sleep onset," *Sleep*, vol. 31, no. 4, pp. 525–33, 2008.

[12] C. De Luca and Z. Erim, "Common drive of motor units in regulation of muscle force," *Trends Neurosci*, vol. 17, no. 7, pp. 299–305, 1994.

[13] A. Fuglevand, D. Winter, and A. Patla, "Models of recruitment and rate coding organization in motor-unit pools," *J Neurophysiol*, vol. 70, no. 6, pp. 2470–88, 1993.

[14] E. Henneman, G. Somjen, and D. Carpenter, "Excitability and inhibitability of motoneurons of different sizes," *J Neurophysiol*, vol. 28, no. 3, pp. 599–620, 1965.

[15] E. Doble, J. Leiter, S. Knuth, J. Daubenspeck, and D. Bartlett Jr, "A noninvasive intraoral electromyographic electrode for genioglossus muscle," *J Appl Physiol*, vol. 58, no. 4, pp. 1378–82, 1985.